Title	Direct observation of mercury amalgamation on individual gold nanorods using spectroelectrochemistry
Authors	Schopf, Carola;Wahl, Amélie;Martín, Alfonso;O'Riordan, Alan;Iacopino, Daniela
Publication date	2016-06-28
Original Citation	Schopf, C., Wahl, A., Martín, A., O'Riordan, A. and Iacopino, D. (2016) 'Direct Observation of Mercury Amalgamation on Individual Gold Nanorods Using Spectroelectrochemistry', The Journal of Physical Chemistry C, 120(34), pp. 19295-19301. doi: 10.1021/acs.jpcc.6b04668
Type of publication	Article (peer-reviewed)
Link to publisher's version	https://pubs.acs.org/doi/abs/10.1021/acs.jpcc.6b04668 - 10.1021/acs.jpcc.6b04668
Rights	© 2016 American Chemical Society. This document is the Accepted Manuscript version of a Published Work that appeared in final form in The Journal of Physical Chemistry C, copyright © American Chemical Society after peer review and technical editing by the publisher. To access the final edited and published work see https://pubs.acs.org/doi/abs/10.1021/acs.jpcc.6b04668
Download date	2024-09-18 23:18:27
Item downloaded from	https://hdl.handle.net/10468/8137

*Tyndall National Institute, Dyke Parade, Cork, Ireland

*Carola Schopf, Amelíe Wahl, Alfonso Martín, Alan O'Riordan, Daniela Iacopino**

Direct Observation of Mercury Amalgamation on Individual Gold Nanorods Using Spectroelectrochemistry

Spectroelectrochemical Cell

A schematic of the spectroelectrochemical cell is shown in Figure S1 together with photographs of the built cell. From bottom to top the spectroelectrochemical cell was constituted by a glass cover slip with a 20 nm ITO coating and immobilised gold nanorods forming the working electrode (Figure S1a). Copper foil tracks were used for external electrical contact of gold nanorods/ITO electrodes. Double adhesive imaging spacers electrically insulated all copper tracks and defined (9 mm inner hole diameter) the exposed active area of the working electrode in the centre of the cover slip (S1b). A platinum wire positioned between the two imaging spacers acted as a pseudo reference electrode. Around the perimeter of the central well a coiled platinum wire served as a counter electrode. A 0.5 mm thick silicone spacer with a 13 mm inner diameter created the main chamber of the cell which was then sealed off by a cover slip after injection of the analyte solution. The cell was then placed into a custom made aluminium holder compatible with the microscope stage to allow for spectroelectrochemical investigation of the mercury - gold nanorod amalgamation process (S1b).

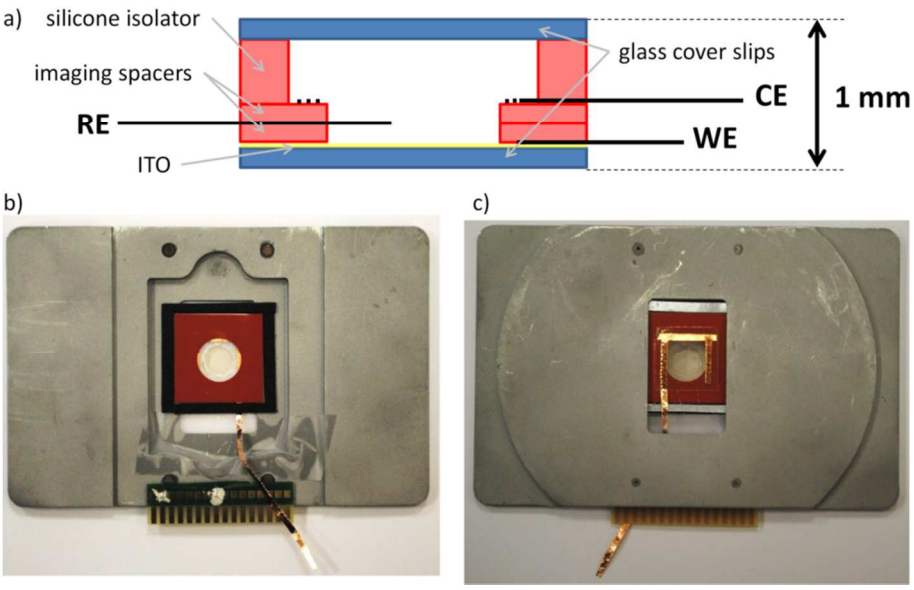

Figure S1: a) Schematic cross section of the designed spectroelectrochemical cell indicating positions of the ITO/gold working electrode (WE), platinum pseudo-reference electrode (RE) and counter electrode (CE). Photographs of the spectroelectrochemical cell mounted in the aluminium holder viewed from b) the top and c) from the bottom.

Gold Nanorod ITO electrode characterisation

In order to verify that Au nanorods were in conductive contact with the ITO substrate non-faradaic charging experiments were carried out. As the decreasing and increasing of free electron density induced by charging of nanorods is expected to result in alteration of nanorod optical signature, non-faradic charging experiments were carried out while monitoring the optical signature of single nanorods.

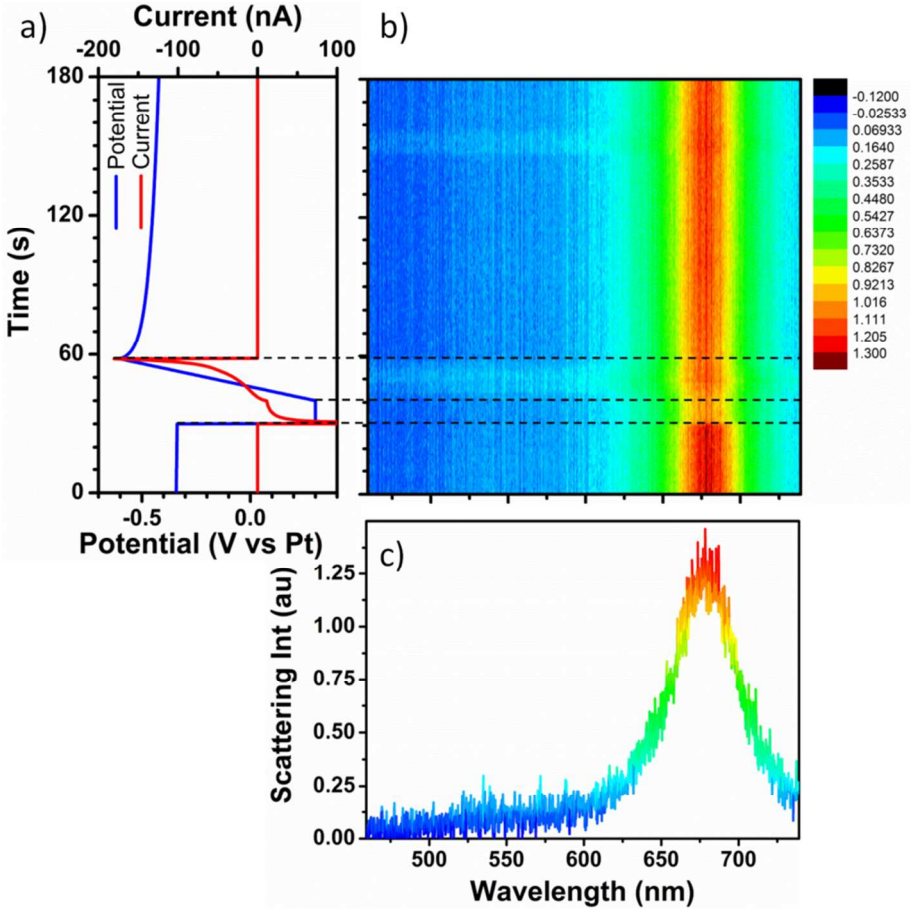

Figure S2: a) Potential and Current curves for a 0.3 V to -0.6V LSV in 0.1 M KCl. b) 2D plot of 180 single nanorod scattering spectra recorded during the LSV. c) Spectrum recorded at 0s as typical example for a single nanorod scattering spectrum showing colour assignment to scattering intensity values.

For this purpose linear sweep voltammetry (LSV) and cyclic voltammetry (CV) were performed in 0.1 M KCl while recording in real time the scattering spectra of a selected single gold nanorod. Figure S1a shows the recorded potential and current during LSV.

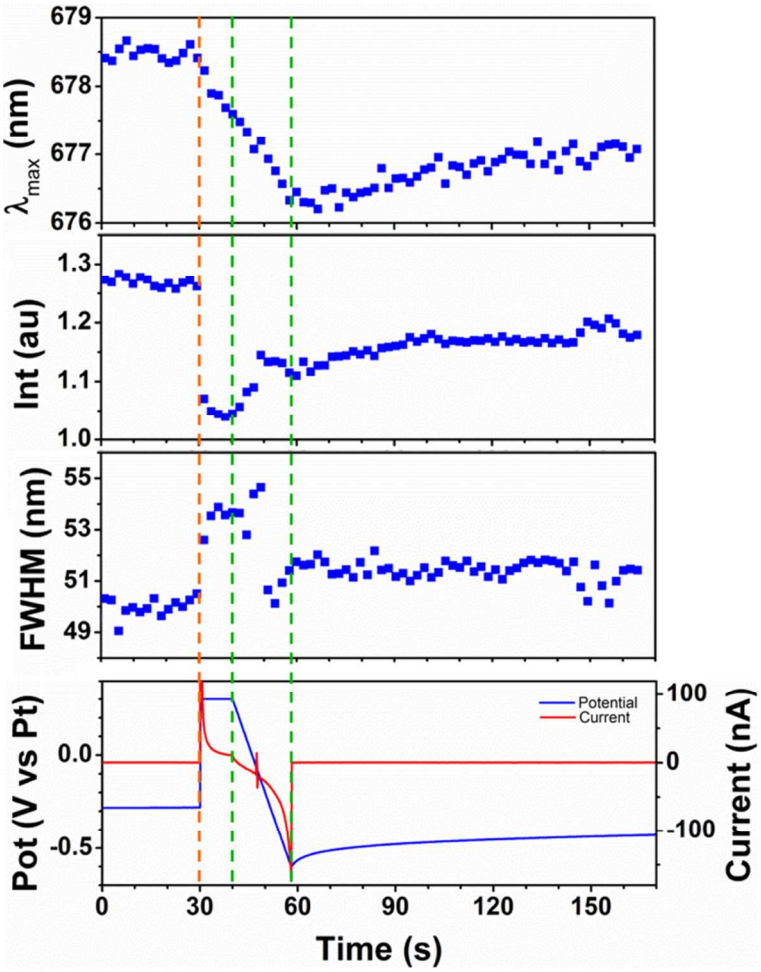

Figure S3: λ_{max}, peak intensity and FWHM values extracted from Lorentzian fits to spectral data correlated with potential and current curves recorded during LSV.

The open cell potential (ocp) was monitored for 30 s, then the potential was held at 0.3 V for 10s before it was scanned linearly to -0.6 V at a rate of 50 mV/s in 10 V steps; finally the ocp was recorded for further 240 s. Throughout the experiment scattering spectra of the nanorod were recorded every second, as shown in Figure S2a displaying all 180 recorded spectra in a 2D

colour map format. As representative example the first scattering spectrum recorded at t=0 is also shown in Figure S2c displaying the assignment of colours to scattering intensity values of the spectra for the colour mapping. By fitting the recorded scattering spectra with a Lorentzian function the peak position λ_{max}, the peak intensity and the full width at half maximum (FWHM) can be extracted. The values for these parameters are plotted in Figure S3. During the first 30 s of ocp scattering spectra λ_{max}, peak intensities and FWHMs remained constant with minor noise fluctuations. During the 10 s of 0.3 V applied potential λ_{max} shifted gradually to shorter wavelengths while the peak intensity dramatically dropped and the FWHM increased significantly. During the linear sweep period (between 40-60 s) λ_{max} further decreased while the peak intensity increased and the FWHM decreased again. Finally, during the following opc period λ_{max} slowly shifted to higher wavelengths again, the peak intensity further recovered towards its initial value and the FWHM remained constant apart from noise fluctuations.

Additionally, non-faradaic charging experiments were carried out using cyclic voltammetry (CV) in 0.1 M KCl. Figure S4 shows the recorded potential and current during CV. The correlated scattering spectra of a selected Au nanorod showed reversible charging/discharging, associated with linear back and forth potential sweeps as displayed in the 2D plot of the 180 scattering spectra recorded during CV. The nanorod charging/discharging associated with potential increase/decrease resulted in corresponding increase/decrease of λ_{max} and FWHM scattering spectra, and decrease/increase of the peak intensity. The above capacitive charging experiments proved that Au nanorods were in conductive contact with the ITO substrate and had the potential to act as active sites for redox reactions.

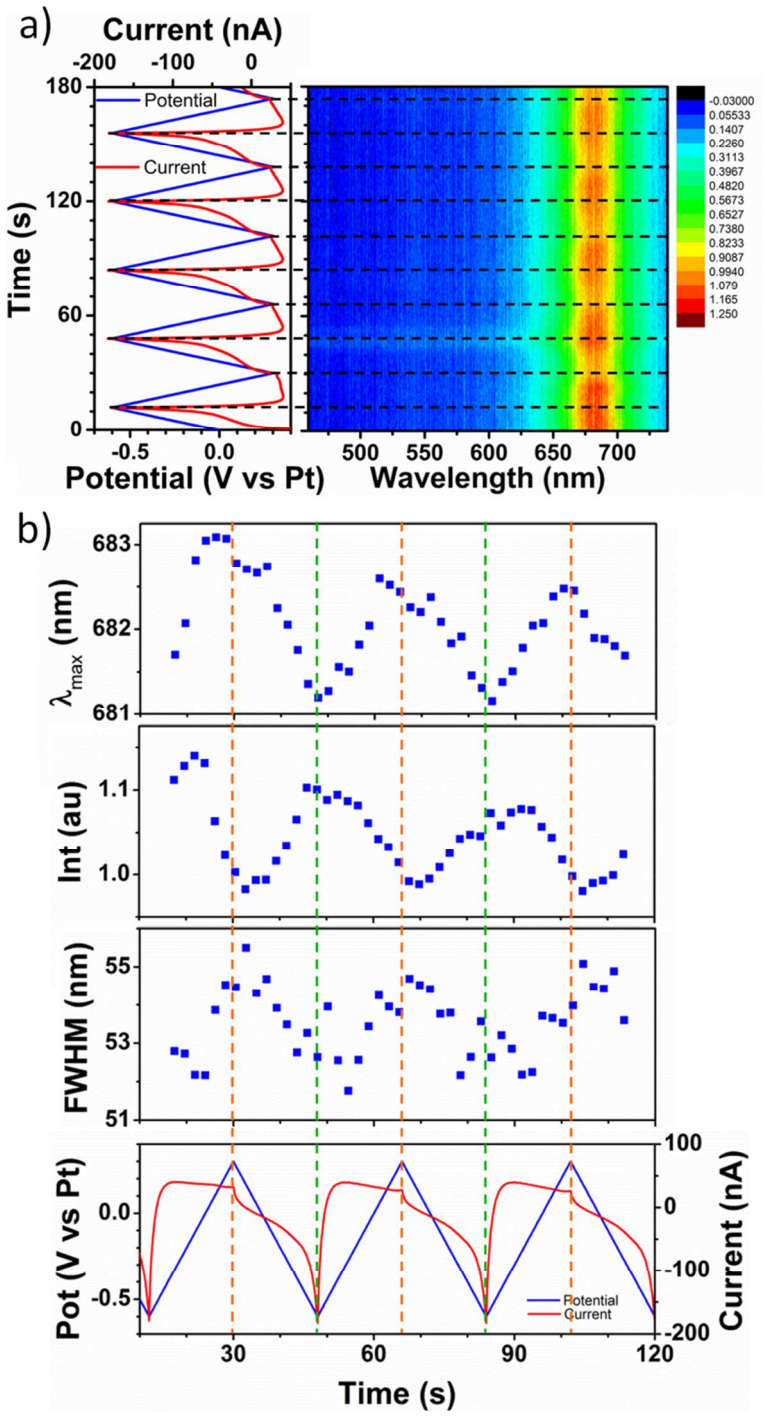

Figure S4: a) Potential and Current curves for a 0.3 V to -0.6V (starting at 0 V) CV in 0.1 M KCl correlated with a 2D plot of 180 single nanorod scattering spectra recorded during the LSV. b) λ_{max}, peak intensity and FWHM values extracted from Lorentzian fits to spectral data correlated with potential and current curves recorded during CV.

Electrochemical Reduction of Hg^{2+} on nanorod/ITO electrodes

Figure S5 shows LSVs for pure supporting electrolyte (0.1 M KCl) and Hg^{2+} containing solutions at an ITO/gold nanorod electrode and at a bare ITO working electrode. In the case of gold nanorod-modified ITO electrode a strong reduction peak was observed at -0.3 V for 5 µM $HgCl_2$ in 0.1 M KCl while no peak was observed in presence of KCl alone (Figure a). Scans over a wider potential window (1 V to -0.6 V, data not shown) displayed no further peaks, thus confirming that the observed peak can be associated to the reduction of Hg^{2+}. The shoulder at -0.1 V could not be assigned to any electrochemical process with certainty. It might be related to the formation of a monolayer of Hg prior to its evolution as a multilayer, or the reduction of Hg^{2+} to Hg_2^{2+} species, which according to the electrochemical series takes place at slightly more positive potentials than the reduction of Hg^{2+} to Hg. The increase of current below ~-0.4 V observed in presence and absence of $HgCl_2$ was attributed to the onset of hydrogen evolution.

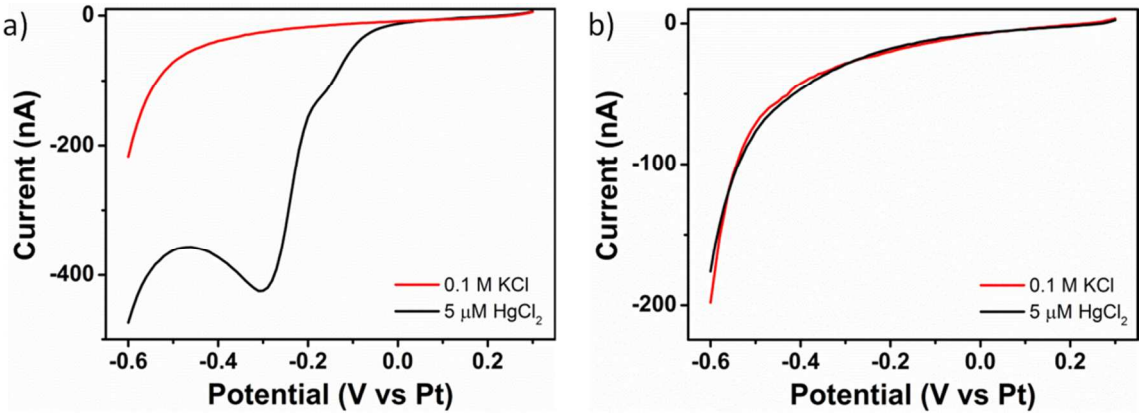

Figure S5: a) LSV in 0.1 M KCl and 0.1 M KCl containing 5 µM $HgCl_2$ on a nanorod modified ITO electrode. b) LSV in 0.1 M KCl and 0.1 M KCl containing 5 µM $HgCl_2$ on a bare ITO electrode.

In contrast, LSVs at bare ITO electrode showed nearly identical curves for the scans in KCl solution with and without 5 μM $HgCl_2$ (Figure b), leading to conclude that, if at all, only very small amounts of Hg^{2+} were reduced in this case. Additionally, the LSVs of KCl at both electrodes were very similar in shape and current magnitude, suggesting that the capacitive charging and the onset of hydrogen evolution mainly took place at the ITO surface, while the Hg^{2+} reduction was confined to the surface of gold nanorods with negligible contributions from the ITO surface.

SEM imaging if ITO/nanorod working electrode

The SEM image of the nanorod/ITO electrode recorded after LSV in presence $HgCl_2$ (Figure S6) revealed partial transition of deposited nanorods to spherical shape, thus confirming the occurrence of amalgamation process associated to the electrochemical reduction of $HgCl_2$. Nanorod AR transitioned from the initial value of 1.9 to 1.2. Such morphological changes correlated well with the marked optical changes observed by darkfield microscopy reported in the main manuscript (Figure 1a-e).

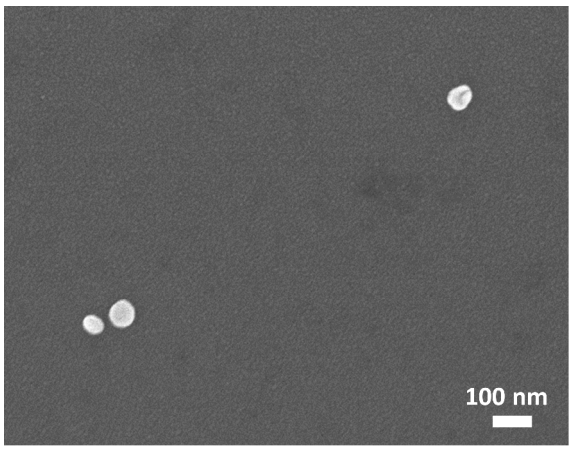

Figure S6. SEM image of a nanorod working electrode after LSV in 0.1 M KCl, 5 μM $HgCl_2$.

Response to multiple linear sweeps

The effect of multiple linear sweeps was also investigated. Figure S7 show single particle scattering images and spectra of one selected nanorod following LSVs and the voltammograms corresponding to three consecutive linear sweeps in 0.1 M KCl containing 5 μM $HgCl_2$. No scattering color change was detected after the first LSV in KCl and before LSV in presence of $HgCl_2$ (7a). However, color transition from red to yellow to green occurred in presence of $HgCl_2$ after further two consecutive LSVs (7a). Accordingly, the position of λ_{max} (671 nm) remained unchanged after the first LSV in KCl (7b, red curve) and before LSV in presence of $HgCl_2$ (7b, green curve) but progressively blue shifted to 590 nm and 536 nm after two consecutive LSVs in presence of $HgCl_2$. Furthermore the three recorded voltammograms displayed different signals. Three consecutive LSVs (Figure S7c) in presence of $HgCl_2$ were characterized by a first large distinct reduction peak at -0.3 V (7c, black curve), a broad peak at -0.28 V (7c, red curve) and a small wave at -0.25V, (7c, blue curve) respectively. As showed in calculations in the manuscript text, the analyte solution was not depleted of mercury ions after one linear sweep. Therefore the overall spectroelectrochemical response was attributed to alteration of the working electrode surface after accumulative deposition of mercury following consecutive sweeps. This in turn was caused by the irreversibility of the mercury deposition process on gold nanorods leading to irreversible formation of amalgamated nanorods due to the high affinity between mercury and gold.

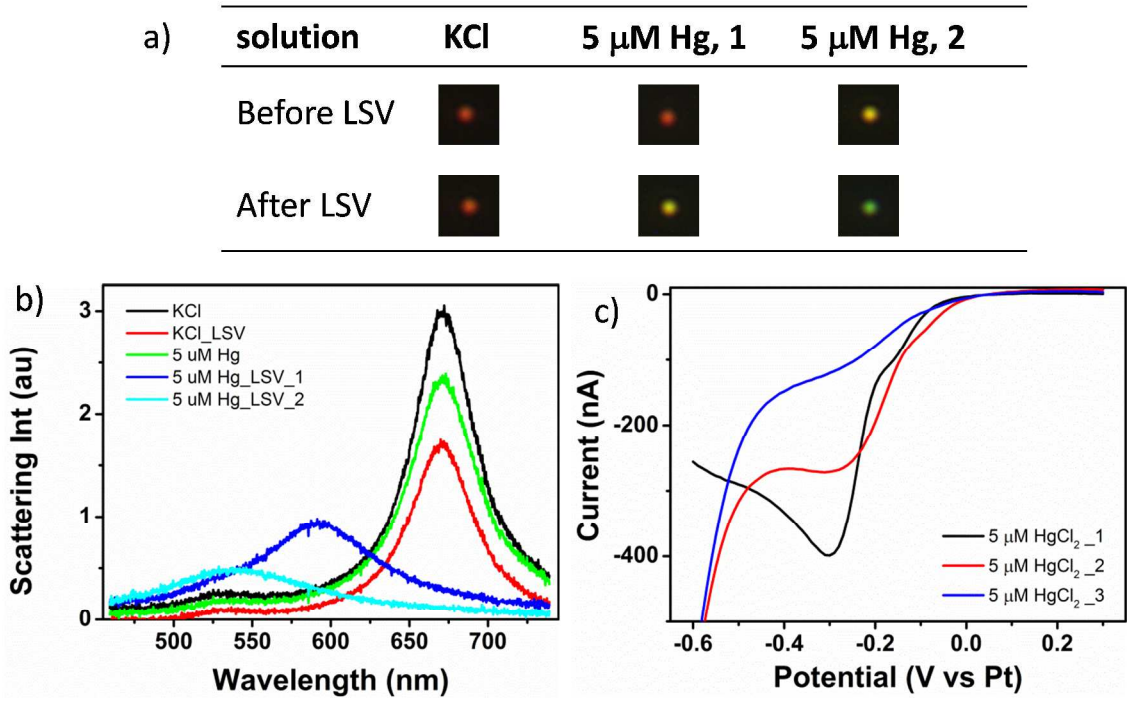

Figure S7. Darkfield images (a) and scattering spectra (b) of a single gold nanorod before and after LSV in KCl and in 0.1 M KCl, 5 μM $HgCl_2$ for two consecutive LSV. c) Voltammograms of three consecutive LSVs in 0.1 M KCl, 5 μM $HgCl_2$.